Numerical Heat Transfer, Part A, 36:725–736, 1999

1040–7782 /99 $12.00 + .00

COMBINED EFFECT OF INERTIA AND A SPANWISE PRESSURE GRADIENT ON FREE CONVECTION FROM A VERTICAL SURFACE IN POROUS MEDIA

D. A. S. Rees
Department of Mechanical Engineering, University of Bath, Bath BA2 7AY, UK

M. A. Hossain
Department of Mathematics, University of Dhaka, Dhaka 1000, Bangladesh

The free convective boundary layer flow induced by a uniform temperature semi-infinite vertical surface embedded in a porous medium is considered. Particular attention is paid to how inertial effects (form drag or Forchheimer) combine with a spanwise pressure gradient to affect the otherwise two-dimensional flow. The resulting flow is three-dimensional but self-similar. The boundary layer equations are supplemented by an algebraic equation governing the magnitude of the spanwise velocity field. The modifications required to solve this problem using the Keller box method are described. It is found that inertial effects serve to inhibit the spanwise flow near the heated surface.

INTRODUCTION

In recent years, interest has developed in the study of natural convection flow in porous media from the surface of various configurations. The first studies were by Cheng and Minkowycz [1] for a vertical heated surface and by Cheng and Chang [2] for a horizontal surface; in both cases the boundary layer flow is self-similar when the surface has a power law surface temperature distribution. Later, Minkowycz and Cheng [3] studied the nonsimilar natural convection flow induced by a vertical heated cylinder embedded in a saturated porous medium using a local similarity method. Subsequently, Merkin [4] reinvestigated the problem posed by Minkowycz and Cheng [3] using an implicit finite difference method, a series expansion method near the leading edge, and an asymptotic analysis far downstream; their analysis was extended to power law surface temperature distributions by Bassom and Rees [5]. However, all these studies were confined to the Darcy flow case only. Extensions to non-Darcy flow using the Forchheimer model of form drag have been undertaken for all of the above configurations. Plumb and Huenefeld [6] considered vertical boundary layer flow, while Rees [7] and Hossain and Rees [8] studied a horizontal surface, and Ingham [9] investigated boundary layer flow over axisymmetric and two-dimensional bodies of arbitrary shape.

Received 22 July 1998; accepted 15 May 1999.
The authors would like to thank one of the referees for comments that improved the presentation of this work.
Address correspondence to Dr. D. A. S. Rees., Department of Mechanical Engineering, University of Bath, Claverton Down, Bath, BA2 7AY UK.

NOMENCLATURE

A, B, C, D, E	coefficients defined in Eq. (15)	x	vertical coordinate
f, F	scaled stream function	y	horizontal cross-stream coordinate
g, G	temperature	z	horizontal spanwise coordinate
$\tilde{g}$	gravity	α	effective thermal diffusivity
Gr	Grashof number	β	volumetric coefficient of isobaric thermal expansion
K	permeability		
$\tilde{K}$	inertia parameter	ΔT	temperature drop ($= T_1 - T_0$)
L	representative length scale	ζ	scaled similarity variable
p	pressure	η	similarity variable
q	fluid flux speed	θ	temperature
Ra	Darcy-Rayleigh number	μ	viscosity
S	scaled spanwise pressure gradient	ρ	density
T	temperature	ψ	stream function
T_0	temperature of ambient medium		
T_1	temperature of heated surface		
u	vertical flux velocity		
v	horizontal cross-stream flux velocity	**Superscripts**	
w	horizontal spanwise flux velocity	$-$	boundary layer variables
W	scaled horizontal spanwise flux velocity	$*$	dimensional variables

For a more complete understanding of transport phenomena in a porous medium, the influence of surface mass flux on Darcian free convection boundary layer flow along both vertical and horizontal surfaces was studied by Minkowycz et al. [10]. Lai and Kulacki [11] and Kumari et al. [12] investigated the self-similar and nonsimilar solutions, respectively, for non-Darcy mixed convection flow on a horizontal surface with power law surface temperature with the further influence of surface mass flux. On the other hand, Hossain and Nakayama [13] investigated the combined effects of the surface mass flux, variable wall temperature, and porous inertia on heat transfer from a vertical cylindrical surface due to non-Darcy free convective flow. Hossain et al. [14] investigated non-Darcy forced convection boundary layer flow over a wedge placed in a saturated porous medium. In Ref. [14], three separate methodologies were employed to solve the governing equations, namely, a series expansion method, the local nonsimilarity method, and an implicit finite difference scheme. All of these papers dealt with the effects of surface suction, but Merkin [15] also considered how the vertical boundary layer is modified by surface blowing.

In the present paper the free convective boundary layer flow induced by a uniform temperature semi-infinite vertical surface embedded in a porous medium is considered. Particular attention is paid to how inertial (form drag or Forchheimer) effects combine with the presence of a spanwise pressure gradient to affect the otherwise two-dimensional flow. The resulting flow is three-dimensional but self-similar and not dependent on the spanwise variable. The boundary layer equations are supplemented by an algebraic equation governing the magnitude of the spanwise velocity field. The modifications required to solve this problem using

the Keller box method are described. It is found that inertial effects serve to inhibit the spanwise flow near the heated surface.

EQUATIONS OF MOTION

A vertical semi-infinite surface is held at the uniform temperature T_1 and is embedded in a fluid-saturated porous medium with ambient temperature T_0, where $T_1 > T_0$. The steady, three–dimensional equations of motion and energy transport are given by

$$u^*_{x^*} + v^*_{y^*} + w^*_{z^*} = 0 \tag{1a}$$

$$u^*\left[1 + \left(\tilde{K}\rho/\mu\right)q^*\right] = -(K/\mu)[\, p^*_{x^*} - \rho\tilde{g}\beta(T - T_0)] \tag{1b}$$

$$v^*\left[1 + \left(\tilde{K}\rho/\mu\right)q^*\right] = -(K/\mu)\, p^*_{y^*} \tag{1c}$$

$$w^*\left[1 + \left(\tilde{K}\rho/\mu\right)q^*\right] = -(K/\mu)\, p^*_{z^*} \tag{1d}$$

$$u^*T_{x^*} + v^*T_{y^*} + w^*T_{z^*} = \alpha(T_{x^*x^*} + T_{y^*y^*} + T_{z^*z^*}) \tag{1e}$$

where subscripts denote partial derivatives and $q^* = \sqrt{(x^*)^2 + (y^*)^2 + (z^*)^2}$. In writing Eqs. (1), it is assumed that the Boussinesq approximation is valid, that boundary effects as modeled by the Brinkman terms are absent, and that the fluid and porous matrix are everywhere in local thermodynamic equilibrium. In the above, x^* is the vertical coordinate, y^* is the horizontal coordinate perpendicular to the heated surface (cross-stream), z^* is the horizontal coordinate parallel to the surface (spanwise), and u^*, v^*, and w^* are the corresponding fluid flux velocities (i.e., macroscopic velocities resulting from averaging the detailed microscopic velocity field over a suitably small representative elementary volume). Other terms are defined in the nomenclature, but it is necessary to point out that $\tilde{K}$ is a dimensional measure of the inertial impedance of the matrix; see Rees [7] and Ergun [16].

The main fluid dynamical aim of this paper is to determine the combined effect of inertia and a spanwise pressure gradient on the free convective boundary layer flow induced by a heated surface, and given that $\rho g\beta\Delta T$ has the same dimensions as that of a pressure gradient, we will assume that there also exists an external pressure gradient of size

$$p^*_{z^*} = -(\rho\tilde{g}\beta\Delta T)S \tag{2}$$

where S is a dimensionless factor measuring the strength of the pressure gradient.

The following nondimensionalizations are introduced:

$$(x^*, y^*, z^*) = L(x, y, z) \tag{3a}$$

$$(u^*, v^*, w^*) = \frac{\alpha}{L}(u, v, w) \tag{3b}$$

$$p^* = (\rho \tilde{g} \beta \Delta T L)(p - Sz) \tag{3c}$$

$$T = T_0 + (\Delta T)\theta \tag{3d}$$

$$q^* = \frac{\alpha}{L} q \tag{3e}$$

where the external pressure gradient as been accounted for explicitly in Eq. (3c). Eqs. (1) reduce to the form

$$u_x + v_y + w_z = 0 \tag{4a}$$

$$u[1 + (\mathrm{Gr}/\mathrm{Ra})q] = -p_x + \mathrm{Ra}\,\theta \tag{4b}$$

$$v[1 + (\mathrm{Gr}/\mathrm{Ra})q] = -p_y \tag{4c}$$

$$w[1 + (\mathrm{Gr}/\mathrm{Ra})q] = -p_z + \mathrm{Ra}\,S \tag{4d}$$

$$u\theta_x + v\theta_y + w\theta_z = \theta_{xx} + \theta_{yy} + \theta_{zz} \tag{4e}$$

The boundary conditions required to complete the specification of the problem are

$$y = 0: \quad v = 0 \quad \theta = 1 \qquad y \to \infty: \quad v, \theta \to 0 \tag{4f}$$

The two nondimensional numbers that appear in Eqs. (4) are

$$\mathrm{Ra} = \frac{\rho \tilde{g} \beta K L (T_1 - T_0)}{\mu \alpha} \qquad \mathrm{Gr} = \left(\frac{\rho}{\mu}\right)^2 K \tilde{K} \tilde{g} \beta (T_1 - T_0) \tag{5}$$

which are the Darcy-Rayleigh number, which is assumed to be very large, and an inertial parameter, which is assumed to take $O(1)$ values. Plumb and Huenefeld [6], in their pioneering work on the effects of inertia on boundary layer flows, term Gr a Grashof number.

There is no reason to suppose that any z variation exists in physically realizable solutions of Eqs. (4), for although we have not proved that the resulting boundary layer flow is stable, it seems very likely that it will be so, given the recent works of Rees [17] and Lewis et al. [18]. Therefore we may set all these z derivatives to zero. The boundary layer equations are found using the substitutions

$$u = \mathrm{Ra}\,\bar{u} \qquad v = \mathrm{Ra}^{1/2}\,\bar{v} \qquad w = \mathrm{Ra}\,\bar{w} \qquad q = \mathrm{Ra}\,\bar{q} \qquad x = \bar{x} \qquad y = \mathrm{Ra}^{-1/2}\,\bar{y} \tag{6}$$

and, given that the flow is two-dimensional, we also introduce the stream function ψ, using

$$\bar{u} = \psi_{\bar{y}} \qquad \bar{v} = -\psi_{\bar{x}} \tag{7}$$

On setting $\mathrm{Ra} \to \infty$ and retaining leading order terms (i.e., on applying the boundary layer approximation), we obtain

$$\psi_{\bar{y}}\left[1 + \mathrm{Gr}\left(\psi_{\bar{y}}^2 + \bar{w}^2\right)^{1/2}\right] = \theta \tag{8a}$$

$$\theta_{\bar{y}\bar{y}} = \psi_{\bar{y}}\theta_{\bar{x}} - \psi_{\bar{x}}\theta_{\bar{y}} \tag{8b}$$

$$\bar{w}\left[1 + \mathrm{Gr}\left(\psi_{\bar{y}}^2 + \bar{w}^2\right)^{1/2}\right] = S \tag{8c}$$

Note that the equation for $\bar{w}$ is algebraic, rather than partial differential, but that $\bar{w}$ is a function of both $\bar{x}$ and $\bar{y}$. It is also necessary to note that our assumptions that Gr and S are $O(1)$ quantities are essential in order to obtain a nontrivial interaction between the effects of inertia and the cross-stream pressure gradient.

The usual similarity transformation may be used (see Ref. [1]), and therefore we substitute

$$\psi = \bar{x}^{1/2} f(\eta) \qquad \theta = g(\eta) \qquad \bar{w} = \bar{w}(\eta) \qquad \eta = \bar{y}/\bar{x}^{1/2} \tag{9}$$

in Eqs. (8) to obtain

$$f'\left[1 + \mathrm{Gr}\,(f'f' + \bar{w}^2)^{1/2}\right] = g \tag{10a}$$

$$g'' + (1/2) fg' = 0 \tag{10b}$$

$$\bar{w}\left[1 + \mathrm{Gr}\,(f'f' + \bar{w}^2)^{1/2}\right] = S \tag{10c}$$

Therefore the flow remains self-similar, although the equation for $\bar{w}$ is algebraic. Equations (10) form a two-parameter system of equations, which may be solved using the Keller box method after suitable modification.

NUMERICAL METHOD

The so-called Keller box method was introduced by Keller [19] and has become widely known through the work of Cebeci and Bradshaw [20]. It was originally devised as an efficient and general means of solving parabolic systems of partial differential equations, such as those that arise in boundary layer theory, and it remains in frequent use today. Generally, the system of partial differential equations is reduced to first-order form, discretized using central differences based at the center of a box formed by neighboring grid lines in both the streamwise and cross-stream directions, and finally, solved using a multidimensional form of the Newton-Raphson method. As the algebraic equations obtained from the discretization process are nonlinear, the Newton-Raphson iteration matrix is the Frechét derivative of the algebraic equations, and it necessarily has a block tridiagonal structure. Thus a block-matrix version of the tridiagonal matrix (or Thomas) algorithm is used. In general, rows need to be interchanged in order to ensure that

the diagonal blocks are nonsingular. The full algorithm is usually implemented by encoding explicitly the entries in the iteration matrix. For small-scale problems, such as the present one, which is a fourth-order system of equations, the programming effort to encode the iteration matrix is not great, although any inaccuracies in coding may be noticed by a poor rate of convergence, or even divergence, since the Newton-Raphson method is usually quadratically convergent. In two recent papers by Rees [21, 22], however, very large systems of equations have been solved, and for those works it was essential to have an alternative means of specifying the iteration matrix. In [21] and [22] a numerical differentiation routine was incorporated into the standard Keller box method so that the iteration matrix could be computed directly from the discretized equations. Although this will necessarily make the execution of the code slower in terms of CPU per case, the greatly reduced code development time more than offsets the reduced speed. It is also noteworthy that the numerical differentiation procedure allows the Keller box method to be transformed very quickly from one based on central differences in the streamwise direction, to one based on backward differences. This latter modification was essential for Rees [22] for reasons of numerical stability but is also a necessary modification for solving sets of ordinary differential equations (ODEs) while performing a parameter sweep.

The present problem is not a set of parabolic partial differential equations but is a third-order set of ODEs supplemented by an algebraic equation. The main numerical aim of this paper is to present the manner in which sets of ODEs (and by implication, sets of partial differential equations) subject to algebraic constraints may be solved using the Keller box method.

But first we need to see why it is necessary to have the algebraic constraint. It is possible to eliminate the square root term from between Eqs. (10*a*) and (10*c*) to obtain $\overline{w}$ explicitly in terms of f and g:

$$\overline{w} = f' S / g \tag{11}$$

which, together with Eq. (10*a*), yields

$$f' \left[g + \mathrm{Gr} \, (g^2 + S^2)^{1/2} |f'| \right] = g^2 \tag{12}$$

although $|f'| = f'$ here, since $f' \geq 0$ everywhere. However, when attempting to find a suitable row arrangement for the iteration matrix when solving Eqs. (10*b*) and (12), it soon becomes apparent that there is no such arrangement for which all the diagonal blocks are nonsingular and well-conditioned. Therefore this form of the governing equations has to be discarded.

It is quite possible to solve Eqs. (10) as they stand, but for code validation purposes, we differentiate Eq. (10*a*) once with respect to η to obtain

$$f'' \left[1 + \mathrm{Gr} \, (f' f' + \overline{w}^2)^{1/2} \right] + \mathrm{Gr} \, f' [f' f'' + \overline{w} \, \overline{w}'] / (f' f' + \overline{w}^2)^{1/2} - g' = 0 \tag{13}$$

Therefore we need to solve Eqs. (13), (10*b*), and (10*c*) subject to $f(0) = 0$, $g(0) = 1$, and $f', g \to 0$ as $\eta \to \infty$. Equation (13) is very complicated, and the specification of the corresponding entries in the iteration matrix would be much more complicated; this again justifies the use of a numerical differentiation routine, as mentioned above.

The equations are reduced to first-order form using

$$a = f \qquad b = f' \qquad c = g \qquad d = g' \qquad e = \overline{w} \tag{14}$$

The resulting five equations may be written in the form,

$$A \equiv a' - b = 0 \tag{15a}$$

$$B \equiv b'\left[1 + \mathrm{Gr}\,(b^2 + e^2)^{1/2}\right] + \mathrm{Gr}\, b(bb' + ee')/(b^2 + e^2)^{1/2} - d = 0 \tag{15b}$$

$$C \equiv c' - d = 0 \tag{15c}$$

$$D \equiv d' + (1/2)\, ad = 0 \tag{15d}$$

$$E \equiv e\left[1 + \mathrm{Gr}\,(b^2 + e^2)^{1/2}\right] - S = 0 \tag{15e}$$

and these equations define A, B, C, D, and E. The equations for A, B, C, and D are discretized halfway between grid points, and E is approximated at the grid points. The reason for the latter is that no boundary conditions are specified for $\overline{w}$, and therefore we must obtain exactly the same number of equations for this variable as we have for any other variable if the modifications to the basic Keller box scheme are to be minimized. The basic η grid ranges from $\eta = 0 = \eta_1$ to $\eta = \eta_{\max} = \eta_N$ over N grid points, which are not necessarily equally spaced. The following notation is defined:

$$C_{i+1/2} = \left(\frac{c_{i+1} - c_i}{\eta_{i+1} - \eta_i}\right) - (d_{i+1} + d_i)/2 \tag{16}$$

and

$$E_i = e_i\left[1 + \mathrm{Gr}\,(b_i^2 + e_i^2)^{1/2}\right] - S \tag{17}$$

The Keller box method is now implemented in the usual fashion (but with the numerical differentiation procedure), choosing S to be the equivalent of the marching variable. Clearly, for each value of S, the equations must be discretized in a such a way that only those terms at the current value of S are involved; this is equivalent to the backward differencing approach mentioned above, since no S derivatives appear in the equations! A little effort is required to show that an appropriate way of arranging the discretized equations for the iterative part of the algorithm is to have the following subvectors placed on the first, ith, and last rows of the right-hand side of the Newton-Raphson scheme:

$$(a_1, c_1 - 1, E_1, B_{3/2}, D_{3/2})^T \tag{18a}$$

$$(A_{i-1/2}, C_{i-1/2}, E_i, B_{i+1/2}, D_{i+1/2})^T \tag{18b}$$

and

$$(A_{N-1/2}, C_{N-1/2}, E_N, b_N, c_N)^T \tag{18c}$$

This arrangement of rows avoids singular submatrix blocks on the diagonal.

NUMERICAL RESULTS, ANALYSIS, AND DISCUSSION

Most of the computations presented here were undertaken using a uniform grid of 401 points lying in the range $0 \leq \eta \leq 40$. The results were compared with the analytical value of $f'(0)$,

$$f'(0) = \frac{2}{1 + \left[1 + 4\,\mathrm{Gr}\,(1 + S^2)^{1/2}\right]^{1/2}} \tag{19}$$

which was obtained from Eq. (12), in order to test that the equations had been encoded correctly and to assess the accuracy of the solutions. In all cases, Eq. (19) was obtained precisely, and grid refinement checks indicated at least four places of accuracy.

It is clear from Eq. (19) that, as either Gr or S increases, the induced streamwise velocity at the surface decreases. In the former case, $f'(0) \sim \mathrm{Gr}^{-1/2} \times (1 + S^2)^{-1/4}$ as $\mathrm{Gr} \to \infty$, whereas in the latter case, $f'(0) \sim \mathrm{Gr}^{-1/2} |S|^{-1/2}$. This reduction in the slip velocity is a consequence of the thickening of the boundary layer and the decreasing ability of buoyancy effects to drive the fluid upward. Indeed, for fixed values of S and asymptotically large values of Gr, it may be shown that $\eta = O(\mathrm{Gr})^{1/4}$ is the boundary layer thickness, while for fixed values of Gr and asymptotically large values of S, we have $\eta = O(S^{1/4})$. It is important to note that nonzero values of S have no effect on the streamwise and cross-stream velocities when $\mathrm{Gr} = 0$; in such cases, the spanwise velocity is entirely decoupled from the rest of the flow field.

No analytical expression is available for $g'(0)$, which is proportional to the surface rate of heat transfer, and therefore we present our numerical solutions for this quantity in Figure 1. The same general trend may be observed there, namely, that the magnitude of $g'(0)$ decreases as either S or Gr increases.

For large values of S a scale analysis of Eqs. (10) shows that $\overline{w} = O(S^{1/2})$, $f = O(S^{-1/2})$, and $\eta = O(S^{1/4})$. From this it is possible to show that

$$g'(0) \sim -0.44375(\mathrm{Gr}\,S)^{-1/4} \qquad S \to \infty \tag{20}$$

where the numerical coefficient is that value of $g'(0)$ that is obtained by solving Eqs. (10*a*) and (10*b*) with $\mathrm{Gr} = 0$. The asymptotic values given by Eq. (20) are also displayed in Figure 1, and the agreement is good, especially when Gr is large. For small values of Gr the approach to the asymptotic state given by Eq. (20) is slow compared with that for larger values of Gr.

For large values of Gr it is not possible to produce as simple a formula as Eq. (20) for the rate of heat transfer because the asymptotic problem reduces to a

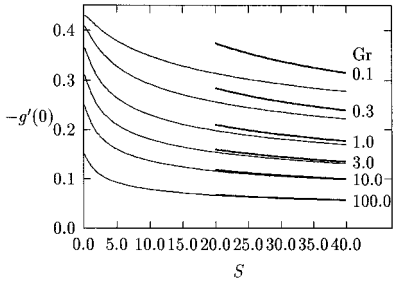

Figure 1. Variation of the surface rate of heat transfer with S for various values of Gr. Heavy curves depict the asymptotic solutions for large values of S.

one-parameter set of equations. On setting $\eta = \mathrm{Gr}^{1/4}\zeta$, $f(\eta) = \mathrm{Gr}^{-1/4}F(\zeta)$, $g(\eta) = G(\zeta)$, and $\overline{w} = \mathrm{Gr}^{-1/2}W$ in Eqs. (10), letting $\mathrm{Gr} \to \infty$, and retaining leading order terms, we obtain the following equations:

$$F_\zeta \left(F_\zeta^2 + W^2\right)^{1/2} = G \tag{21a}$$

$$G_{\zeta\zeta} + \tfrac{1}{2}FG_\zeta = 0 \tag{21b}$$

$$W\left(F_\zeta^2 + W^2\right)^{1/2} = S \tag{21c}$$

which were solved using the methodology described in the previous section. A list of values of $G_\zeta(0)$ as a function of S is given in Table 1. The rate of heat transfer is now given by

$$g'(0) \sim \mathrm{Gr}^{-1/4}\, G_\zeta(0) \tag{22}$$

for asymptotically large values of Gr. Again, good agreement with the computed data is obtained, as confirmed by the entries in Table 1. The values of $G_\zeta(0)$ are also displayed in Figure 2, where we see that increasing inertia effects as S increases causes a reduction in the surface rate of heat transfer.

Table 1. Values of $G_\zeta(0)$ and $g'(0)$ for selected values of S together with the respective asymptotic values given by Eq. (22)

S	$G_\zeta(0)$	$g'(0)$ at $\mathrm{Gr} = 100$	$\mathrm{Gr}^{-1/4}G_\zeta(0)$
0.1	−0.49033	−0.15019	−0.15506
0.2	−0.48399	−0.14843	−0.15305
0.5	−0.45955	−0.14144	−0.14532
1.0	−0.42033	−0.12996	−0.13292
2.0	−0.36705	−0.11410	−0.11607
5.0	−0.29592	−0.092542	−0.093578
10.0	−0.24937	−0.078236	−0.078858
20.0	−0.20980	−0.065980	−0.066345
50.0	−0.16687	−0.052612	−0.052769

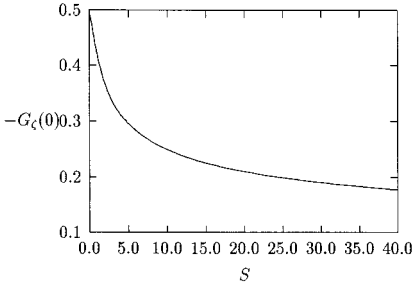

Figure 2. Variation of $G_\zeta(0)$ with S for asymptotically large values of Gr.

Finally, it is of interest to note how the vertical buoyancy-induced motion affects the spanwise fluid velocity, which in the absence of convective effects, is uniform. Equation (10) may be manipulated to yield

$$\overline{w} = \frac{2S}{1 + \left[1 + 4\,\mathrm{Gr}\,(S^2 + g^2)^{1/2}\right]^{1/2}} \tag{23}$$

from which we may deduce that

$$\frac{2S}{1 + \left[1 + 4\,\mathrm{Gr}\,(S^2 + 1)^{1/2}\right]^{1/2}} = \overline{w}(0) \leq \overline{w}(\eta) \leq \overline{w}(\infty) = \frac{2S}{1 + [1 + 4\,\mathrm{Gr}\,|S|]^{1/2}} \tag{24}$$

In Figure 3 we display how $(\overline{w}(\infty) - \overline{w}(0))$ varies with Gr and S, since this value is a measure of the retardation of the spanwise flow brought about by the combined action of inertia and the buoyancy-induced flow. Note that this function of Gr and S has a maximum value of 0.068605 when $\mathrm{Gr} = 1.599640$ and $S = 0.515538$; these values were obtained by setting both the Gr and S partial derivatives of $(\overline{w}(\infty) - \overline{w}(0))$ to zero and iterating using a two-dimensional Newton-Raphson scheme.

The relative retardation of the spanwise flow is shown in Figure 4, where the variation with Gr and S of $(\overline{w}(\infty) - \overline{w}(0))/\overline{w}(\infty)$ is displayed. The relative retardation is strongest when Gr is large and S is small, and it decreases monotonically as either Gr decreases or S increases. We note that the relative retardation is, strictly

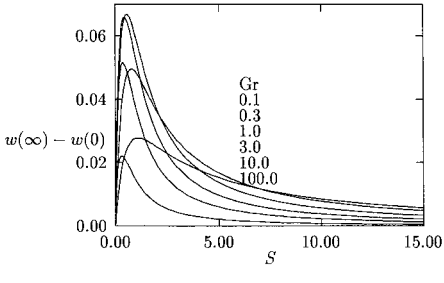

Figure 3. Variation with S of the spanwise velocity retardation, $w(\infty) - w(0)$, for various values of Gr.

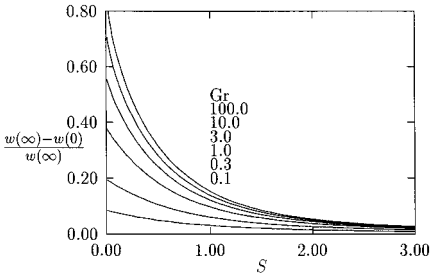

Figure 4. Variation with S of the relative retardation of the spanwise velocity, $[w(\infty) - w(0)]/w(\infty)$, for various values of Gr.

speaking, not defined when $S = 0$, for then $\overline{w} = 0$, but it has a well-defined limit:

$$\lim_{S \to 0} \frac{\overline{w}(\infty) - \overline{w}(0)}{\overline{w}(\infty)} = \frac{\sqrt{1 + 4\,\mathrm{Gr}} - 1}{\sqrt{1 + 4\,\mathrm{Gr}} + 1} \tag{25}$$

CONCLUSION

When the flow in a porous medium is governed by Darcy's law, the buoyancy-induced flow from a vertical surface and the spanwise drift induced by a horizontal pressure gradient are entirely independent of one another. However, when inertial effects are present, the mechanisms interact. The spanwise flow serves to inhibit the effectiveness of the buoyancy forces, and the boundary layer thereby thickens, and the rate of heat transfer decreases. The upward convection also inhibits the spanwise fluid motion, and it is retarded within the thermal boundary layer.

In this paper we have undertaken a mainly numerical analysis of this self-similar boundary layer flow. The equations were of the form of an ordinary differential system supplemented by an algebraic constraint. The means were presented by which the Keller box method may be used to solve such systems and, by implication, parabolic partial differential systems with an algebraic constraint.

REFERENCES

1. P. Cheng and W. J. Minkowycz, Free Convection About a Vertical Flat Plate Imbedded in a Porous Medium with Application to Heat Transfer from a Dike, *J. Geophys. Res.*, vol. 82, pp. 2040–2044, 1977.
2. P. Cheng and I.-D. Chang, Buoyancy Induced Flows in a Saturated Porous Medium Adjacent to Impermeable Horizontal Surfaces, *Int. J. Heat Mass Transfer*, vol. 19, pp. 1269–1272, 1976.
3. W. J. Minkowycz and P. Cheng, Free Convection About a Vertical Cylinder Embedded in Porous Medium, *Int. J. Heat Mass Transfer*, vol. 19, pp. 805–813, 1976.
4. J. H. Merkin, Free Convection From a Vertical Cylinder Embedded in a Porous Medium, *Acta Mech.*, vol. 62, pp. 19–28, 1986.
5. A. P. Bassom and D. A. S. Rees, Free Convection From a Heated Vertical Cylinder Embedded in a Fluid-Saturated Porous Medium, *Acta Mech.*, vol. 116, pp. 139–151, 1996.

6. O. A. Plumb and J. C. Huenefeld, Non-Darcy Natural Convection from Heated Surfaces in Saturated Porous Media, *Int. J. Heat Mass Transfer*, vol. 24, pp. 765–768, 1981.
7. D. A. S. Rees, The Effect of Inertia on Free Convection from a Horizontal Surface Embedded in Porous Medium, *Int. J. Heat Mass Transfer*, vol. 39, pp. 3425–3430, 1996.
8. M. A. Hossain and D. A. S. Rees, Non-Darcy Free Convection Along a Horizontal Heated Surface, *Transport Porous Media*, vol. 29, pp. 309–321, 1997.
9. D. B. Ingham, The Non-Darcy Free Convection Boundary Layer on Axisymmetric and Two-Dimensional Bodies of Arbitrary Shape, *Int. J. Heat Mass Transfer*, vol. 29, pp. 1759–1763, 1986.
10. W. J. Minkowycz, P. Cheng, and F. Mialem, The Effect of Surface Mass Transfer on Buoyancy Induced Darcian Flow Adjacent to a Horizontal Heated Surface, *Int. Commun. Heat Mass Transfer*, vol. 12, pp. 55–65, 1985.
11. F. C. Lai and F. A. Kulacki, The Influence of Surface Mass Flux on Mixed Convection over Horizontal Places in Saturated Porous Media, *Int. J. Heat Mass Transfer*, vol. 33, pp. 576–579, 1990.
12. M. Kumari, I. Pop, and G. Nath, Non-Similar Boundary Layer for Mixed Convection Flow About a Horizontal-Surface in a Saturated Porous Medium, *Int. J. Eng. Sci.*, vol. 28, pp. 253–263, 1990.
13. M. A. Hossain and A. Nakayama, Non-Darcy Free Convection Flow Along a Vertical Cylinder Embedded in a Porous Medium with Surface Mass Flux, *Int. J. Heat Fluid Flow*, vol. 14, pp. 385–390, 1993.
14. M. A. Hossain, N. Banu, and A. Nakayama, Non-Darcy Forced Convection Boundary Layer Flow Over a Wedge Embedded in a Saturated Porous Medium, *Numer. Heat Transfer Part A*, vol. 26, pp. 399–414, 1994.
15. J. H. Merkin, Free Convection Boundary Layers in a Saturated Porous Medium with Lateral Mass Flux, *Int. J. Heat Mass Transfer*, vol. 21, pp. 1499–1504, 1978.
16. S. Ergun, Fluid Flow Through Packed Columns, *Chem. Eng. Proc.*, vol. 48, pp. 84–94, 1952.
17. D. A. S. Rees, Nonlinear Wave Stability of Vertical Thermal Boundary Layer Flow in a Porous Medium, *J. Appl. Math. Phys. (ZAMP)*, vol. 44, pp. 306–313, 1993.
18. S. Lewis, A. P. Bassom, and D. A. S. Rees, The Stability of Vertical Thermal Boundary Layer Flow in a Porous Medium, *Eur. J. Mech. B Fluids*, vol. 14, pp. 395–408, 1995.
19. H. B. Keller, Numerical Methods in Boundary Layer Theory, *Annu. Rev. Fluid Mech.*, vol. 10, pp. 417–433, 1978.
20. T. Cebeci and P. Bradshaw, *Physical and Computational Aspects of Convective Heat Transfer*, Springer, New York, 1984.
21. D. A. S. Rees, Three-Dimensional Free Convection Boundary Layers in Porous Media Induced by a Heated Surface with Spanwise Temperature Variations, *Trans. ASME J. Heat Transfer*, vol. 119, pp. 792–798, 1997.
22. D. A. S. Rees, Free Convection Boundary Layer Flow from a Heated Surface in a Layered Porous Medium, *J. Porous Media*, vol. 2, pp. 39–58, 1999.